Elsevier Editorial System(tm) for Remote Sensing of Environment
Manuscript Draft

Manuscript Number: RSE-D-16-01436

Title: Validating SMAP SSS with in situ measurements

Article Type: Research Paper

Keywords: SMAP, Sea Surface Salinity, Argo float, moored buoy

Corresponding Author: Dr. Wenqing Tang,

Corresponding Author's Institution: Jet Propulsion Laboratory

First Author: Wenqing Tang

Order of Authors: Wenqing Tang; Alexandre Fore; Simon Yueh; Tong Lee; Akiko Hayashi; Alejandra Sanchez-Franks; Brian King; Dariusz Baranowski; Justino Martinez

Highlights

- Sea surface salinity retrieved from SMAP radiometer is validated with in situ data
- SMAP achieved 0.2 PSU accuracy on a monthly basis in tropics comparing with Argo OI
- SMAP can track large salinity changes occurred within a month consistent with buoy
- SMAP SSS retrieved in Mediterranean sea and BOB assessed with ship TSG and Argo STS

Validating SMAP SSS with in situ measurements

Wenqing Tang[1], Alexander Fore[1], Simon Yueh[1], Tong Lee[1], Akiko Hayashi[1],
Alejandra Sanchez-Franks[2], Brian King[2], Dariusz Baranowski[1], and Justino Martinez[3]

[1]Jet Propulsion Laboratory, California Institute of Technology, Pasadena, CA, USA
[2]National Oceanography Centre, Southampton, UK
[3]Institut de Ciències del Mar, CSIC, Barcelona, Spain

Abstract

Sea surface salinity (SSS) retrieved from SMAP radiometer measurements is validated with in situ salinity measurements collected from Argo floats, tropical moored buoys and ship-based thermosalinograph (TSG) data. SMAP SSS achieved accuracy of 0.2 PSU on a monthly basis in comparison with Argo gridded data in the tropics and mid-latitudes. In tropical oceans, time series comparison of salinity measured at 1 m by moored buoys indicates that SMAP can track large salinity changes occurred within a month. Synergetic analysis of SMAP, SMOS and Argo data allows us to identify and exclude erroneous jumps or drift in some real-time buoy data from assessment of satellite retrieval. The resulting SMAP-buoy matchup analysis leads to an average standard deviation of 0.22 PSU and correlation coefficient of 0.73 on weekly scale; the average standard deviation reduced to 0.17 PSU and the correlation improved to 0.8 on monthly scale. SMAP L3 daily maps reveals salty water intrusion from the Arabian Sea into the Bay of Bengal during the Indian summer monsoon, consistent with the daily

measurements collected from floats deployed during the Bay of Bengal Boundary Layer Experiment (BoBBLE) project field campaign. In the Mediterranean Sea, the spatial pattern of SSS from SMAP is confirmed by the ship-based TSG data.

Key Words: SMAP, Sea Surface Salinity, Argo float, moored buoy

1. Introduction

The spacebased observation of sea surface salinity (SSS) is crucial for the global water cycle studies. The L-band microwave technology has been used to measure the sea surface salinity (SSS) on two satellite missions: the NASA's Aquarius [Le Vine et al., 2007; Lagerloef et al., 2008] and the ESA's Soil Moisture and Ocean Salinity (SMOS) [Kerr et al., 2010; Font et al., 2010]. The third satellite carrying L-band instruments, the NASA Soil Moisture Active Passive (SMAP) observatory, is designed to measure the soil moisture over land [Entekhabi et al., 2010]. Although the primary goal of SMAP is over land, its measurements can also be used to retrieve SSS.

The measurement principle is based on the L-band microwave sensitivity to water salinity, which influences the water dielectric constant and consequently the sea surface emissivity measured as surface brightness temperature (T_B) by radiometer. To accurately retrieve SSS from measured T_B, other factors which also contribute to the surface emissivity need to be accurately accounted for through the so-called "roughness correction". This is achieved through a geophysical model function (GMF) that links the excess surface emissivity to ancillary geophysical parameters, including surface wind speed, direction, significant wave height (SWH), and sea surface temperature (SST). The L-band radar on board of Aquarius played a significant role in the roughness correction as implemented in the combined active and passive (CAP) retrieval algorithm [Yueh et al., 2013; Yueh et al., 2014; Tang et al., 2013; Tang et al. 2015]. The challenge for the operational SMAP SSS retrieval is that it has to rely on radiometer measurements only, after the unfortunate failure of SMAP radar in July 2015, a few months after launch.

The algorithm to retrieve SSS from SMAP radiometer data has been developed at the Jet Propulsion Laboratory (JPL) [Fore et al., 2016]. Analyzing available SMAP and matchup ancillary data, it is found that SMAP T_B well corroborates the Aquarius GMFs for wind speed up to at least 40 m s^{-1} [Yueh et al., 2016]. Therefore, the roughness correction which removes excess surface emissivity from SMAP-measured T_B is currently based on the Aquarius radiometer GMF. The JPL SMAP T_B-only processing uses a maximum-likelihood method to minimize the objective function, which is the square sum of the differences between measured and modeled T_B for each "flavor" (i.e. H-fore, H-aft, V-fore, and V-aft) [Eq. (1) in Fore et al. 2016]. An additional term is included in the objective function to constrain the wind speed within a certain range of ancillary wind speed from the National Centers for Environmental Prediction (NCEP). The salinity is unconstrained except to restrict the valid retrieval between 0 and 40 PSU (practical salinity unit). The SMAP SSS product is available for publicly access (ftp://sealion.jpl.nasa.gov/pub/outgoing/smap/v3.0 or ourcoean.jpl.nasa.gov).

In this paper, we validate JPL SMAP SSS product by comparison with in situ measurements, which are described in Section 2. Validation results are presented in Section 3 and conclusion given in Section 4.

2. Data

The SMAP SSS product analyzed in this study is the version v3.0 Level 3 (L3) data produced by the radiometer T_B-only processing [Fore et al., 2016]. The SMAP Level 2 (L2) SSS and wind speed are retrieved at each of the salinity-wind-cell (SWC) defined along the satellite swath with 1624x76 cells along/cross track per satellite revolution. The L2 data covers global ocean in 8 days with a spatial resolution of ~40 km. There are two

L3 products, monthly and 8-days, both on 0.25°x0.25° grid. The 8-days product is created daily by averaging 8 days of L2 data centered at noon UTC (Coordinated Universal Time) of the day with a search radius of 45 km and Gaussian weighting half-power distance of 30 km.

The Argo array has approximately 3700 floats in the global ocean measuring salinity and temperature profiles [Roemmich and the Argo Team, 2009], with data made freely available by the International Argo Program (see Acknowledgement for data links). We use two objectively interpolated (OI) gridded monthly Argo dataset produced, respectively from the Scripps Institution of Oceanography (SIO) (http://www.argo.ucsd.edu/Gridded_fields.html) and from the Asia-Pacific Data-Research Center (APDRC) of the International Pacific Research Center (IPRC) at the University of Hawaii (http://apdrc.soest.hawaii.edu). The SMAP L3 monthly data is compared with Argo OI salinity at the shallowest depth (2.5 m) produced using individual float measurements within 5 m from the surface.

The moored buoy arrays provide salinity measurements close to the surface (~ 1m) at high temporal resolution in tropical oceans, which include the Tropical Atmosphere Ocean (TAO)/TRITON array in the Pacific [McPhaden, 1995; McPhaden et al., 1998], the Pilot Research Moored Array in the Tropical Atlantic (PIRATA) [Servain et al., 1998; Bourles et al., 2008], and the Research Moored Array for Africa-Asian-Australian Monsoon Analysis and Pre- diction (RAMA) in the Indian Ocean [McPhaden et al., 2009]. The buoy salinity sensors record temperature and conductivity data at 10-minute intervals, which are used to compute hourly averaged salinity with an accuracy of 0.02 PSU [Freitag et al., 1999]. The depths at which salinity measurements are available vary with buoy locations. In this study, we only use the salinity measurements obtained within 1 m from the surface to assess whether SMAP L3 SSS accurately depict the changes occurred at weekly time scales to complement the analysis based on monthly Argo-gridded products.

We also explore other in situ salinity measurements in the SMAP period particularly in coastal oceans and marginal seas to complement Argo floats and moored buoys. One such source is the salinity data collected by ships assembled by the Global Ocean Surface Underway Data (GOSUD) Project (http://gosud.org) under the Intergovernmental Oceanographic Commission (IOC). Specifically valuable to this study is the large amount of salinity data made available by GOSUD in the Mediterranean Sea where SMAP appears to be able to provide SSS retrievals. We also examined the in situ measurements in the Mediterranean Sea available from the Copernicus (HCMR), an earth observing data center under the European Commission (http://copernicus.eu).

Another special data set recently made available to us is from the Bay of Bengal Boundary Layer Experiment (BoBBLE) project field campaign, which took place June-July 2016 [Matthews et al., 2015]. During this field campaign, 7 Argo floats were deployed in the southern Bay of Bengal along 8°N, between 85.3°E and 89°E. Of particular interest to this study is the daily near surface salinity measurements from the BoBBLE floats equipped with SeaBird (SBE) 41-CP Conductivity, Temperature and Depth (CTD) sensor and Surface Temperature Salinity (STS) sensor, which is a secondary free-flushed conductivity sensor used in conjunction with the CTD for extending the temperature and salinity measurements through the sea surface [Larson et al., 2008]. The STS returns very high-resolution salinity profile with multiple measurements at 0.1 dbar pressure increment in the top one meter from the surface. For this study, we average measurements obtained at pressure less than 0.5 dbar.

SMOS SSS, which was validated [Boutin et al, 2012; Boutin et al., 2016], is used as an independent dataset for comparison in this study. We obtained SMOS salinity data from the Ocean Salinity Expertise Center (CECOS) of the CNES-IFREMER, France. SMOS L3 gridded data is available in 10 Days/monthly composites. SMOS data used in this study is the “research” product before May 2015, and “operational” product afterwards.

3. Results

Figure 1 presents the monthly SSS maps of May 2015 for SMAP, Aquarius, SMOS and SIO Argo. The large-scale features of the salinity fields agree very well

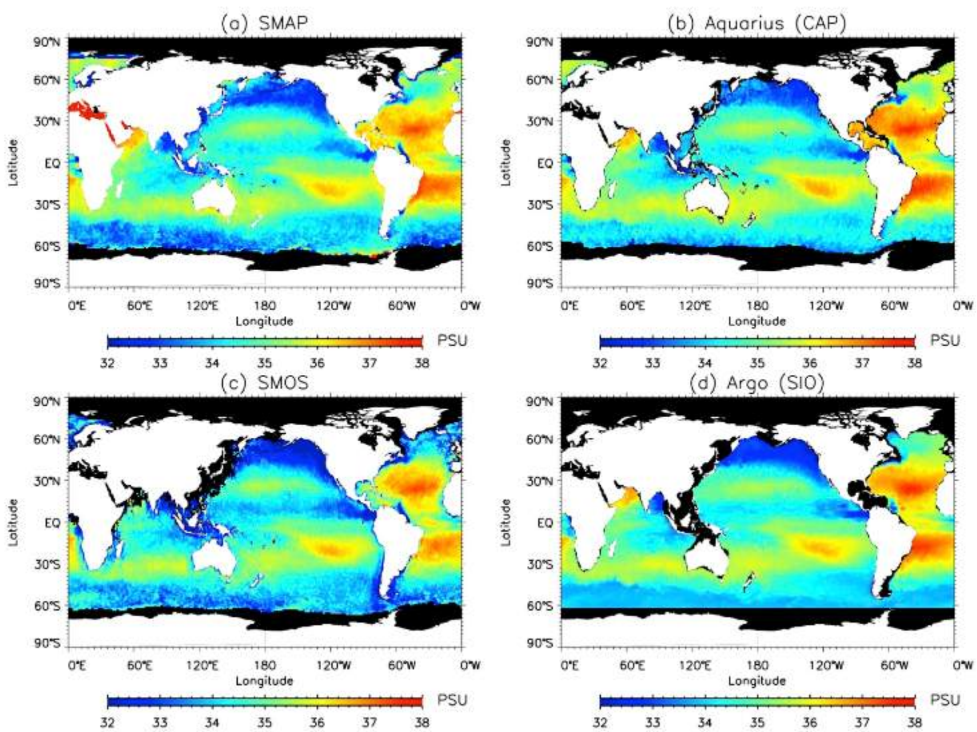

Figure 1. Global maps of sea surface salinity from (a) SMAP, (b) Aquarius (CAP), (c) SMOS and (d) Argo from SIO for the month of May 2015.

between satellites and Argo. We note some new details that SMAP SSS can provide close to land due to its higher spatial resolution than Aquarius and Argo and better built-in radio frequency interference (RFI) detection than Aquarius and SMOS [Mohammed et al., 2016]. Many places where no valid data from Aquarius or SMOS gridded products or Argo OI products, SMAP appears to depict reasonable SSS structure, for example, the extremely salty Mediterranean, Red Sea and the northern tip of the Arabian Sea, the fresh

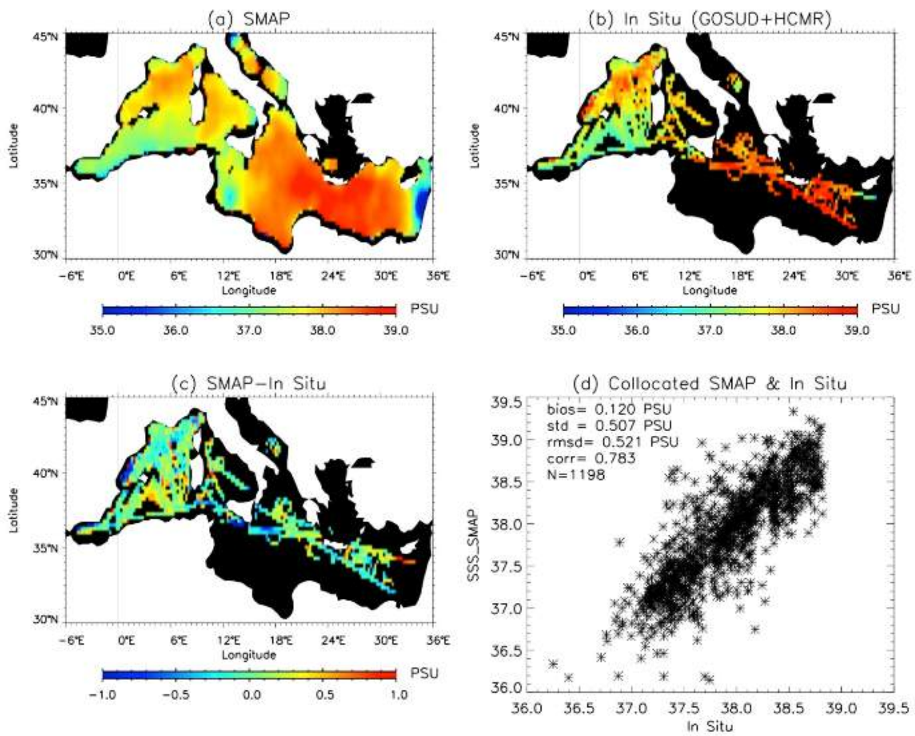

Figure 2. Sea surface salinity in the Mediterranean Sea from (a) SMAP and (b) in situ measurements bin-averaged on 0.25°grid for the period from April 1, 2015 to September 30, 2016. (c) The difference of SMAP minus in situ. (d) Scatter plot of SMAP vs. in situ over collocated grid points.

water on the west side of Pacific along the Kuroshio current, the northward diffusion of the Amazon river runoff plume, and the major river outflows into the coastal regions of Gulf of Mexico [Fournier et al., 2016].

The potential of SMAP for SSS retrieval in the Mediterranean Sea is indicated in Fig. 2. The known regions with persistent RFI are on the eastern part of the Mediterranean adjacent to Syria, Lebanon and Israel and the coast of Libya near Tripoli (See Fig. 13 in Mohammed et al., 2016), which cause lower than expected SMAP salinities (color coded as light or deep blue in Fig. 2a). Searching through the GOSUD database, we found more than 300,000 sea surface salinity measurements from TSG along ship trajectories in the Mediterranean Sea for the period from April 2015 to Sept. 2016, most of them concentrated in the western Mediterranean with two tracks across the basin. We also found some glider and moored buoy data from the Copernicus marine database, which extended the in situ data coverage in the eastern Mediterranean Sea. Combining data from GOSUD and Copernicus, we created the daily bin-average of the in situ data in the domain on 0.25°x0.25° grid. Figure 2 shows the mean SSS from SMAP L3 and in situ data averaged over the period from April 2015 to Sept. 2016. SMAP SSS agrees reasonably well with in situ, depicting the relatively fresh water in the western Mediterranean in Balearic Sea, with increased salinity moving eastward into Tyrrhenian Sea, and becoming extremely salty along the tracks from Sicily to Suez Canal. The correlation between SMAP and ship data over collocated grid points is 0.78 with bias of 0.12 PSU and the standard deviation and Root Mean Square Difference (RMSD) of about 0.5 PSU (Table 1).

Table 1. Statistical differences between SMAP L3 daily SSS and in situ data in the Mediterranean.

In situ	Bias	Standard deviation	RMSD	Correlation
GOSUD/HMCR	0.12	0.51	0.52	0.78
Argo	-0.29	0.50	0.58	0.70
Argo-Zone 1	0.02	0.47	0.47	0.55
Argo-Zone 2	-0.78	0.41	0.89	0.11
Argo-Zone 3	-0.48	0.39	0.62	0.33

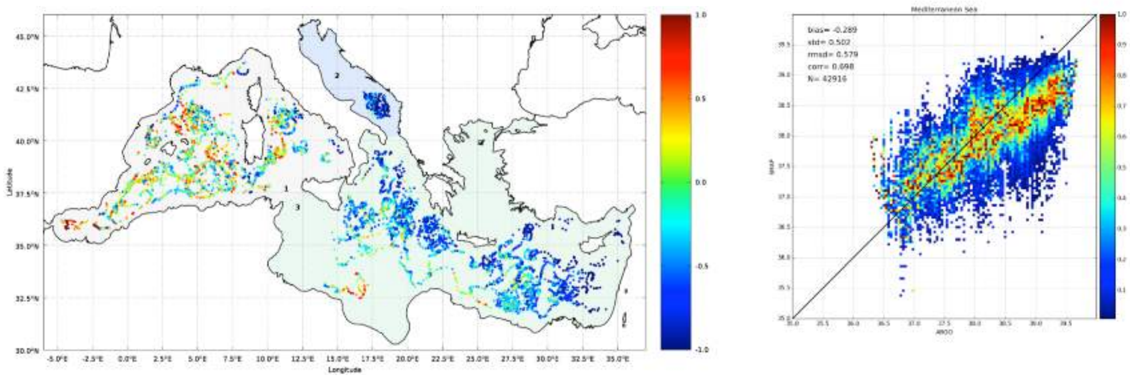

Figure 3. Comparison of SMAP L3 daily and Argo SSS in the Mediterranean during April 4, 2015 and April 3, 2016. (a) Difference map and (b) Density plot. The Mediterranean Sea is divided in the three zones indicated in the figure: Occidental region (zone 1), Adriatic Sea (zone 2) and oriental region (zone 3). Only measurements meeting the constraint: Q1 - 1.5 x IQR < | SMAP -Argo | < Q3 + 1.5 x IQR are used to compute statistics. Q1 and Q3 are the first and third quartile and IQR is the interquartile range (IQR=Q3-Q1). Measurements out of this range are considered as outliers,The data from the whole year are used to compute outliers.

We have compared the daily SMAP L3 SSS with Argo SSS (closest to surface, cut-off at 10m and collocated with 0.25°x0.25° grid cell within 8 days) in the Mediterranean Sea during one year (from April 4, 2015 until April 3, 2016). This is a region strongly affected by RFI. Nevertheless, only a 2.8% of the SMAP-Argo comparisons can be considered as outliers [Tukey, 1977] and are mainly concentrated in the Levantine basin and in the south of the Adriatic Sea (Fig. 3a). By neglecting outlier measurements, the correlation between SMAP and Argo profiles data is about 0.70 with bias of -0.29 PSU, the standard deviation about 0.50 and RMS difference of about 0.58 (Fig. 3b). These values are consistent with the statistical differences from GOSUD and HCMR data (Table 1). It is worth noting that the Argo distribution is conditioned by the bathymetry, showing a lack of measurements in the Sea of Sicily and the Aegean Sea.

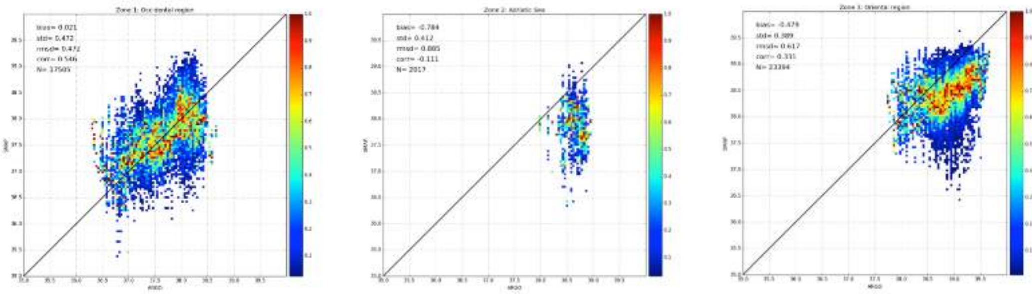

(a) Zone 1 (b) Zone 2 (c) Zone 3

Figure 4. Density plot of SMAP L3 daily maps in front of the corresponding ARGO values for the three regions of the Mediterranean Sea. Data correspond to the period from April 4, 2015 to April 3, 2016.

Three regions can be identified depending on the differences between SMAP and Argo. These regions are shown in Fig. 3a. Inspection of this figure shows that bias of occidental (zone 1) and oriental (zone 3) regions are different, being larger in the oriental one. In the oriental region SMAP provides smaller salinity values than Argo. This difference between three zones is quantified in Fig. 4. The bias in the occidental part is very small (0.02 PSU) with a standard deviation and an RMSD of 0.47, whereas the values of the bias, standard deviation and RMSD increase in the oriental region (-0.48, 0.39 and 0.62, respectively). The cause of this difference could be the concentration of RFI sources in the oriental Mediterranean which is larger than in the occidental region. The comparison in the Adriatic Sea (zone 2) provide poor results (bias of -0.78, RMSD of 0.88 and correlation of -0.11), probably due to the fact that it is a coastal sea and land contamination effects are difficult to correct. A future adjustment of the SMAP RFI mitigation algorithms and land contamination correction could provide better values in zones 2 and 3.

3.1 Comparison with global monthly gridded Argo data

We compare the monthly SMAP L3 SSS with Argo gridded salinity from SIO and APDRC for the period from April 2015 to September 2016. Fig. 5 shows the global

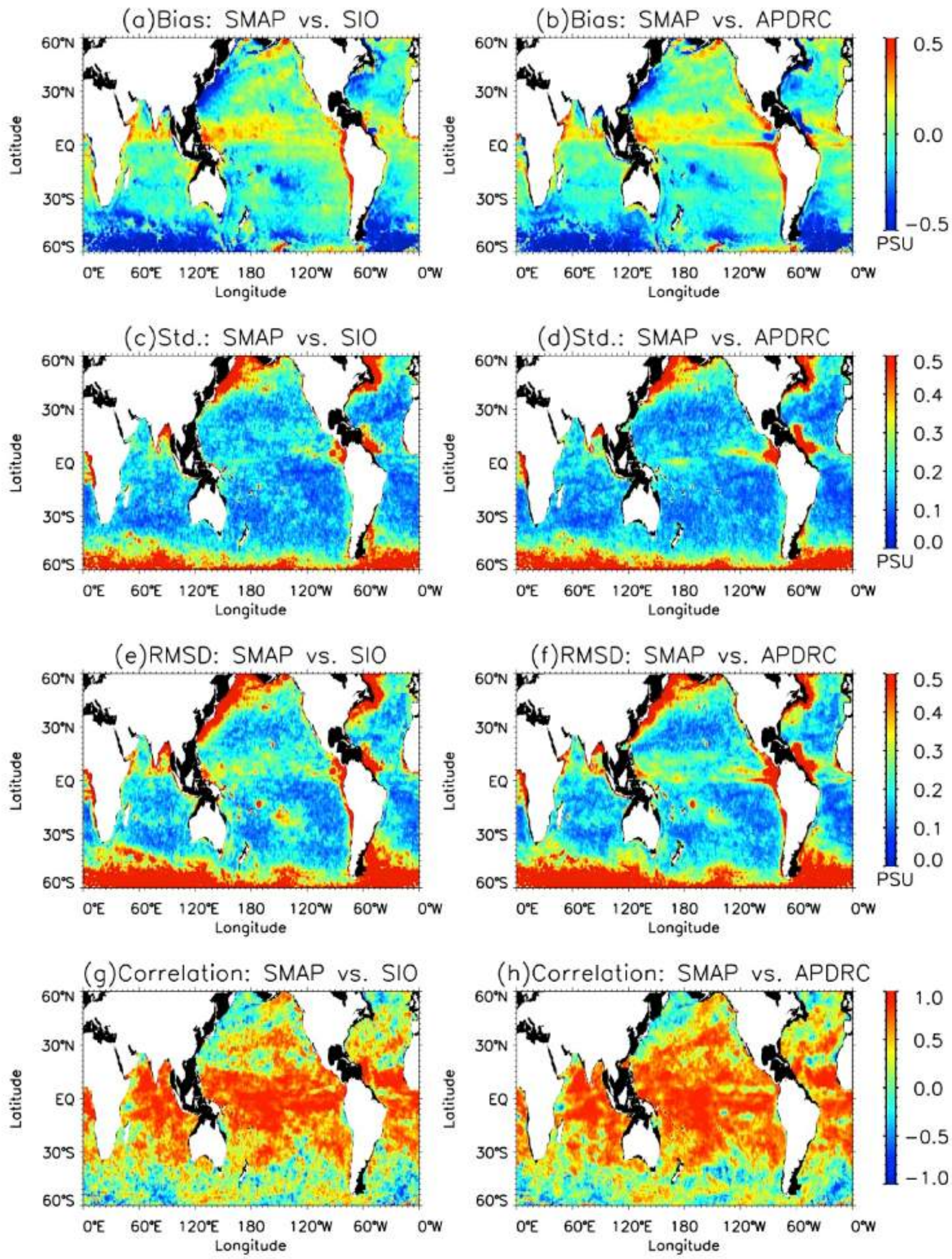

Figure 5. Comparison of SMAP SSS with monthly Argo from SIO (left) and APDRC (right): (a & b) Biases, (c & d) standard deviation, (e & f) RMS difference and (g & h) correlation coefficients.

maps of the mean, standard deviation and Root-Mean-Square (RMS) difference of SMAP minus Argo and their correlation coefficients. In the majority part of the tropical oceans away from the coast, SMAP show small error (< 0.2 PSU) and high correlation (> 0.7) with respect to (w.r.t.) Argo data.

We can identify several regions where there are noticeable large differences between SMAP and Argo OI products. First in the high latitudes (40° poleward) there is large RMSD or standard deviation (> 0.5 PSU) coincident with low correlation (< 0.5). In addition to large instrument measurement error and significantly reduced L-band radiometer sensitivity to salinity signal in cold water, this may also be caused by the degradation in performance of T_B-only retrieval algorithm under the influence of strong wind and high wave without the use of radar data to assist the roughness correction of excess surface emissivity.

Second, large RMS difference are observed in the regions adjacent to land, particularly noticeable along the west coast of Africa and South America, east of North America and Asia, and near Amazon. The substantial negative bias in the coastal oceans of China could be the result of un-mitigated RFI [Mohammed et al., 2016]. Part of those differences could be caused by the error in Argo OI products due to the under-sampling by Argo floats in regions significantly influenced by the spatiotemporal variability associated with boundary currents, river plumes, upwelling, etc.. Along the South America coast near Chili, although RMSD (Fig. 5e & f) is large but the standard deviation (Fig.5c & d) is less than 0.2 PSU. This may suggest error caused by the bias due to the residual error in land contamination correction on SMAP's radiometer data.

Third area with large difference is where there could be significant near surface salinity stratification, such as in the Eastern Pacific Fresh Pool (EPFP) where Argo OI error is small but RMSD/std are large. This is because satellite measures salinity at 1-2 cm near the surface while the majority of Argo floats were turned off within 2-5 m near the surface. Discrepancy is expected between salinity measured by satellite and Argo particularly under persistent rainy conditions [Boutin et al., 2015; Tang et al. 2014].

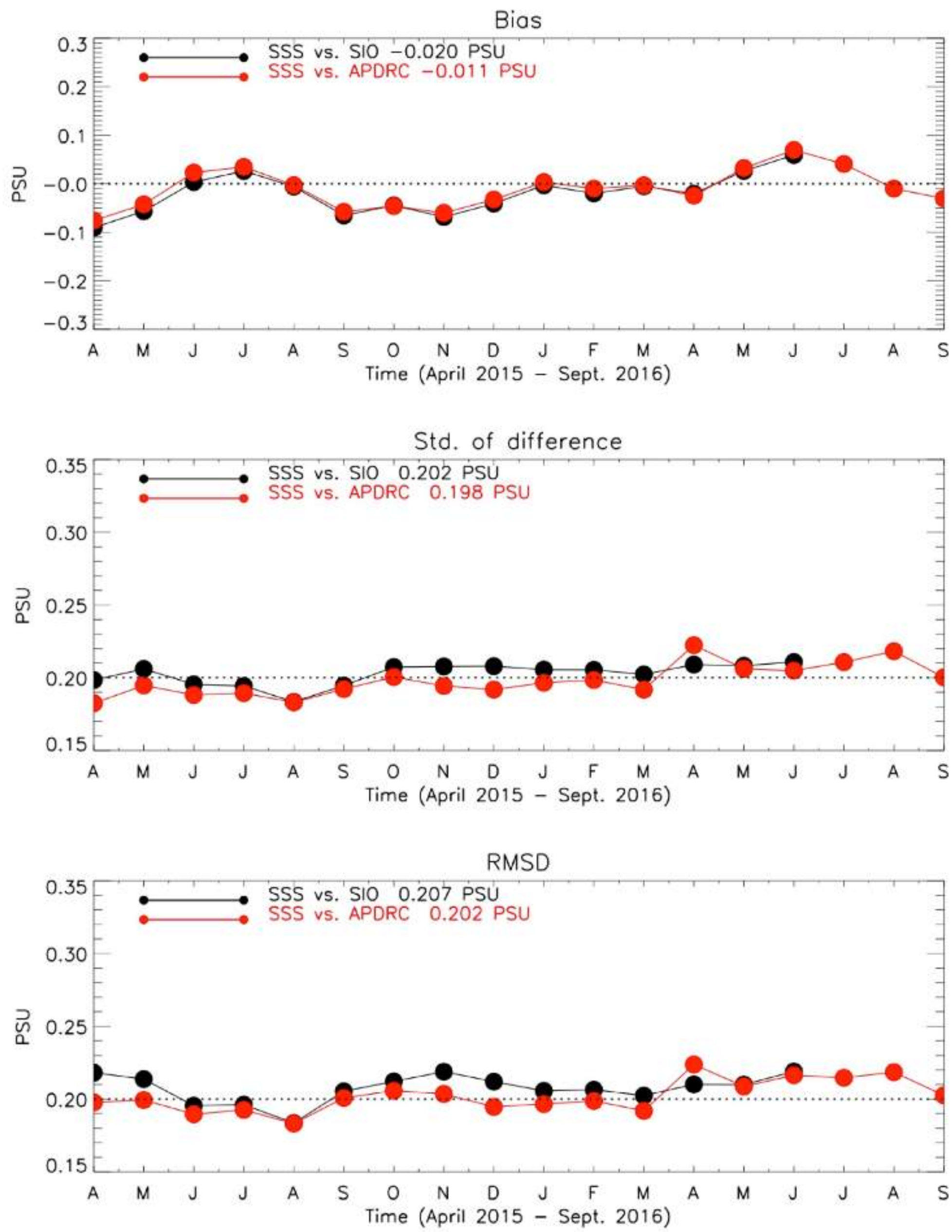

Figure 6. Monthly mean (top), standard deviation (middle) and RMS difference (bottom) between SMAP and Argo from SIO (black) and APDRC (red).

In summary, the comparison with Argo monthly gridded data identified regions where (1) satellite retrieval needs improvements (high latitudes), (2) Argo-gridded data is unreliable to be used for assessment (coastal regions), and (3) SMAP SSS differ from salinity measured by Argo due to near-surface stratification. Excluding those areas, we obtain the monthly error assessment between 40°S and 40°N latitudes as shown in Fig. 6. Averaged over the whole period, the bias between SMAP and Argo is near zero with RMS difference around 0.2 PSU.

3.2 Comparison with moored buoys in the tropics

Moored buoy arrays in tropical oceans provide daily salinity measurements at 1 m depth. Daily sampling of buoy data allows us to validate the SMAP data at weekly-biweekly time scale. We extract the time series of data from L3 SMAP and SMOS products at each buoy locations, with a 7-day moving average applied to the time series of each collocation. As an example, Fig. 7 illustrates the time series at the TAO buoy located at 5°N, 95°W and the RAMA buoy at 0°N, 90°E. It demonstrates that SMAP and SMOS SSS products agree well with each other and depict salinity fluctuations very close to the buoy 1 m salinity. Particularly interesting is that SMAP SSS not only closely agrees with buoy data in depicting the more than 2 PSU freshening peaked in Feb. 2016 at TAO buoy and Nov. 2015 at RAMA buoy, respectively, but also the timing of rapid fluctuations during the course of salt recovering afterwards. The monthly APDRC and SIO SSS in general corroborate the mean of the SMAP and SMOS SSS. However, they missed or underestimated the fluctuations with time scales shorter than about two months, which are signals that SMAP, SMOS, and mooring data show reasonable agreement. Note that there is a time-varying bias of about 0.1 to 0.5 PSU between APDRC and SIO

(a)

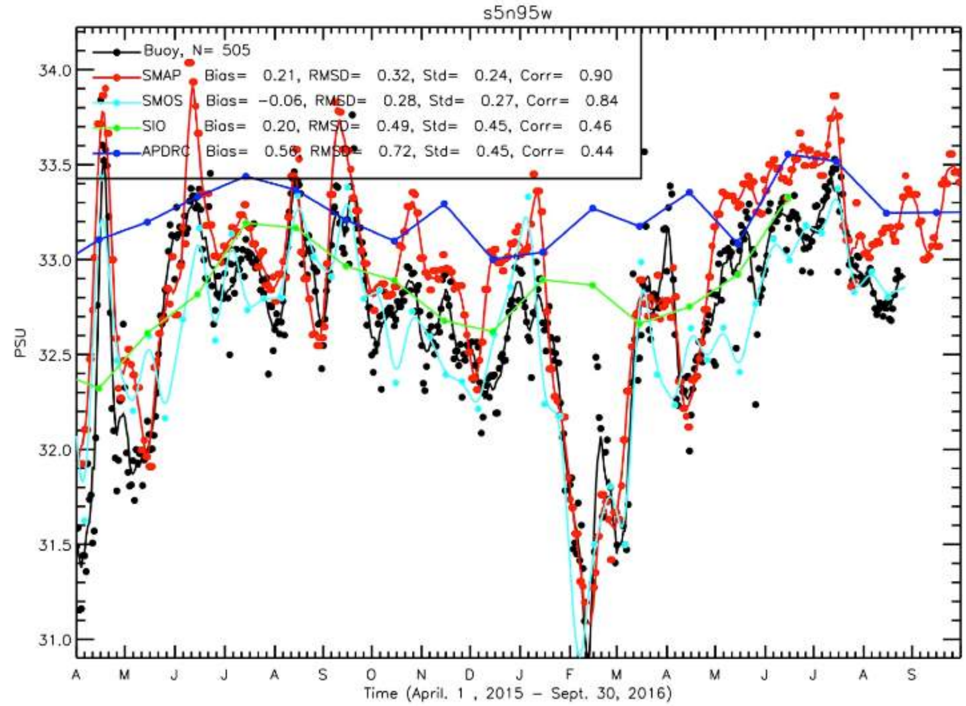

(b)

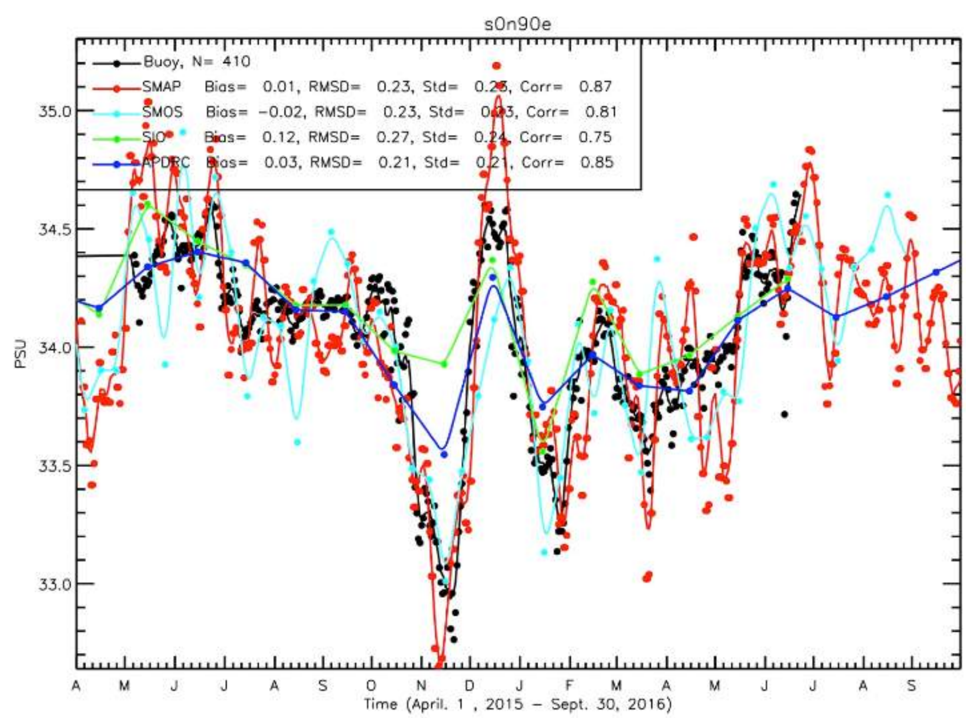

Figure 7. Time series of buoy salinity at 1m depth (black) and collocated SMAP (red) and SMOS (cyan) SSS at (a) TAO buoy location 5°N, 95°W and (b) RAMA buoy location 0°N, 90°E, from April 1, 2015 to Sept. 30, 2016, with 7-day moving average applied, over plotted with monthly Argo data from SIO (green) and APDRC (blue).

at 5°N, 95°W, indicating the uncertainty of Argo-gridded products. The agreement between SMAP, SMOS and buoy SSS demonstrates that SMAP salinity has very good skill to track large change of salinity at about weekly time scale.

We examined the daily 1 m salinity measured at each moored buoy locations from TAO, PIRATA and RAMA arrays. There are total of 97 buoys each with at least 100 daily records collocated with SMAP period. Figure 8 shows the color-coded means, standard deviations, RMS differences and Pearson correlation coefficients between SMAP and buoy. Note the number of collocated pairs between buoy and SMAP varies with locations. SMAP SSS generally agree well with buoys, with temporal correlation at 77 out of 97 buoys locations exceeding 0.6, all of which are statistically significant with p-value less than 0.001.

There are several buoy sites where large biases and RMSD are observed, including the three locations along 180° in the central Pacific, a few locations in the eastern equatorial Pacific fresh pool and in the BOB along 90°E. At these locations, RFI contamination is not likely to be the main error source as indicated by the RFI probability maps [Mohammed et al., 2016]. We suggest two possible causes for the large discrepancy observed. First it may reflect the expected difference between the point-wise in situ measurements and the satellite observations that represent the averages over its footprints [Vinogradova and Ponte, 2013, Boutin et al. 2015]. For example for the several RAMA buoys along 90°E, the agreement between SMAP and buoys are excellent at three southern locations away from the land (1.5°S, 0°, and 4°N) with RMSD ~0.2 PSU and correlation ~ 0.8, but moving northward into BOB the discrepancy becomes larger with RMSD increased to 0.4 PSU and correlation reduced to 0.6. It is likely that in the BOB where SSS structure is dominated by small spatial variability under the influence of river runoffs and meso- and submesoscale variability, there can be a larger difference between the spatial average for satellite measurements with the footprint (~ 40km) and point

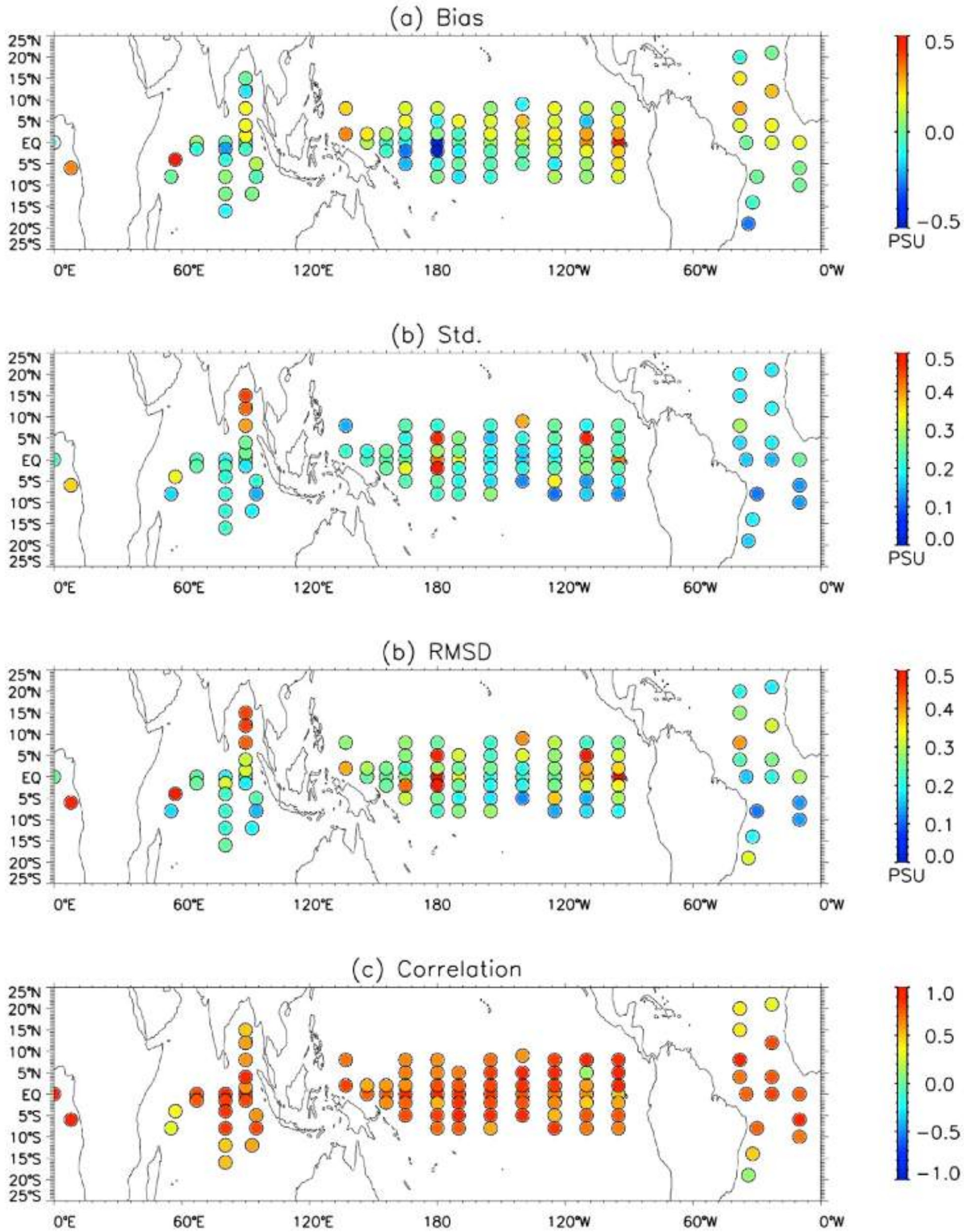

Figure 8. Comparison of SMAP SSS with salinity measured by moored buoys at 1 m depth: (a) Biases, (b) standard deviation, (c) RMS difference and (d) correlation coefficients.

measurements by buoy.

The second possibility is malfunctioning of buoy salinity sensor and the corrupted real time data were not flagged. One such example is the time series of TAO buoy at 5°N, 110°W (Fig.9a), where the real time 1-m salinity from buoy agrees with SMAP and SMOS SSS until Dec. 2015 (the delayed-mode buoy salinity data that have better quality-control flags are not yet available). After Dec. 2015, the mooring salinity became progressively higher. This increase in mooring salinity is inconsistent with the satellite SSS (from SMAP and SMOS) or the Argo products (SIO and APDRC). While buoy salinity drifted away from satellite data by about 1 PSU, it is also interesting to note that the buoy SSS remained to have temporal variation with similar amplitude to SMAP and SMOS. Another example is at TAO location 5°S, 125°W where buoy data suddenly jumped by more than 1 PSU in Sept. 2015 and stay higher than satellite and Argo measurements for the following six months. After March 2016, the buoy salinity values returned to the level agree with all other measurements after the salinity sensor was replaced on March 5, 2016 (Karen Grissom, National Buoy Data Center, personal communication). Clearly, the large standard deviation of the SMAP and buoy differences are essentially caused by the large discrepancy during those periods when buoy data showed suspicious abnormal behavior.

(a)

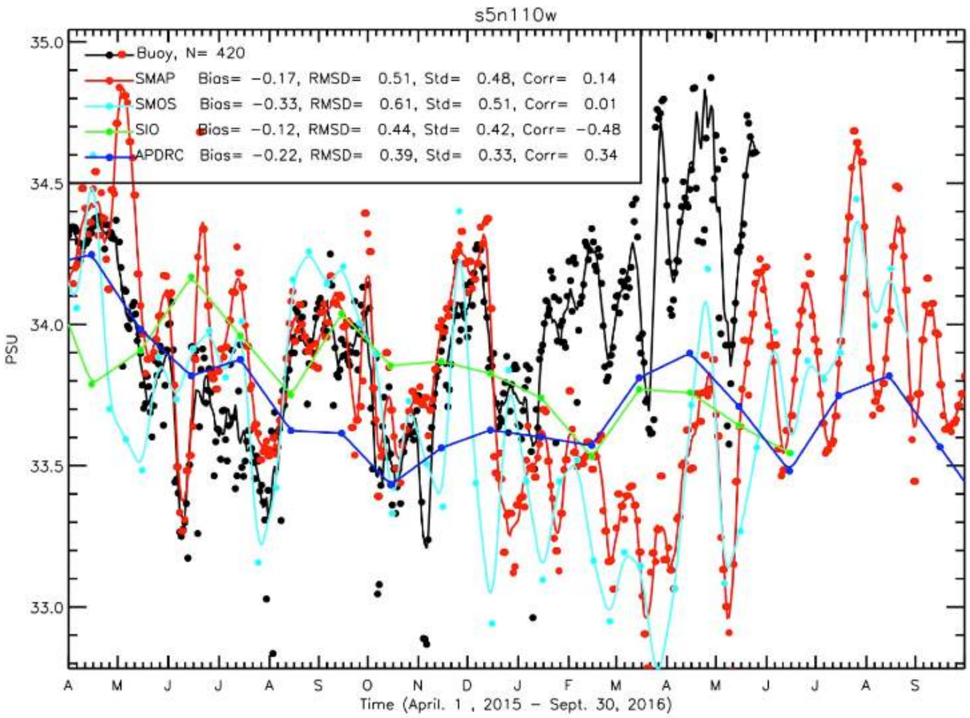

(b)

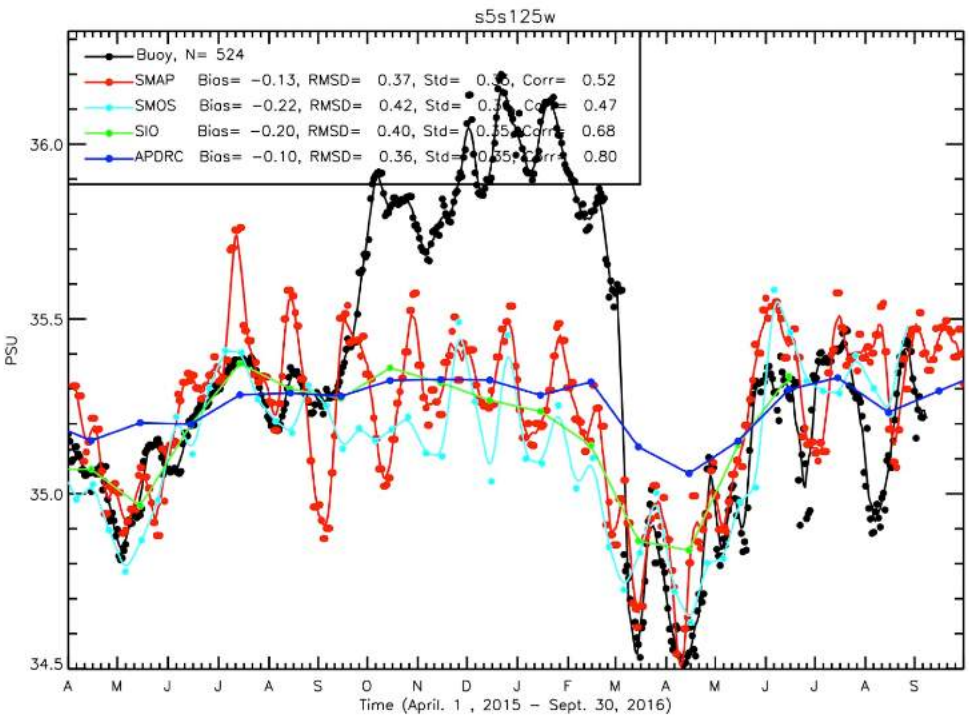

Figure 9. Time series of buoy salinity at 1m depth (black) and collocated SMAP (red) and SMOS (cyan) SSS at TAO buoy location (a) 5°N, 110°W and (b) 5°S, 125°W from April 1, 2015 to Sept. 30, 2016, with 7-day moving average applied, over plotted with monthly Argo data from SIO (green) and APDRC (blue).

Table 2. Statistical differences between SMAP L3, SMOS, Argo from SIO, Argo from APDRC and salinity measured at 1 m by moored buoys.

Dataset	7-day average				30-day average			
	Bias	Standard deviation	RMSD	Correlation	Bias	Standard deviation	RMSD	Correlation
SMAP	0.07	0.22	0.26	0.73	0.05	0.17	0.22	0.80
SMOS	-0.15	0.26	0.26	0.63	-0.16	0.22	0.32	0.71
$ARGO_{SIO}$	0.04	0.19	0.21	0.72	0.03	0.16	0.19	0.79
$ARGO_{APDRC}$	0.03	0.20	0.24	0.66	0.03	0.17	0.21	0.71

After inspecting the time series of all 97 buoys, we found 10 of them have large drift or jump in the 1-m salinity time series, in disagreement with SMAP, SMOS and Argo from SIO or APDRC. These suspicious buoy data, most likely due to malfunctioned mooring salinity sensors (Meghan Cronin, NOAA/Pacific Marine Environmental Laboratory, personal communication), were excluded from SMAP SSS assessment. As listed in Table 2, the bias, standard deviation and RMS difference averaged over the remain 87 buoys are 0.07, 0.22 and 0.26 PSU on 8-day (~weekly) scale and reduces to 0.05, 0.17 and 0.22 PSU on monthly scale (with 30-days moving average applied). Table 2 also summarizes similar statistical comparisons between moored buoys with SMAP, SMOS, Argo from SIO and APDRC respectively. Averaged over 87 buoys, SMAP and Argo products show small biases and similar statistics. The standard deviation and RMSD between SMAP and buoy is slightly higher than that between Argo and buoy by less than 0.05 PSU, while the correlation between SMAP and buoy is slightly better than Argo-gridded on both weekly and monthly scales.

The ability of satellite SSS to identify suspicious mooring salinity data as discussed in relation to Fig. 9 suggests that satellite SSS can be used to perform real-time quality control (QC) of mooring salinity data. While Argo OI products can also be potentially used for this purpose, these products missed or underestimated many shorter-term fluctuations (as discussed earlier). This, compounded by the smaller amount of real-time Argo data volume, limits the potential utility of Argo data for real-time QC of mooring salinity.

3.3 Comparison with STS floats in BOB

Figure 10 shows STS salinity on top of SMAP L3 SSS from July 2 to August 12, 2016, the period when BoBBLE STS data is available. Collocated data is shown in six consecutive plots, each represents one week of SMAP and STS measurements. The daily STS data are matched up with the closest SMAP L3 grid point and over plotted on the

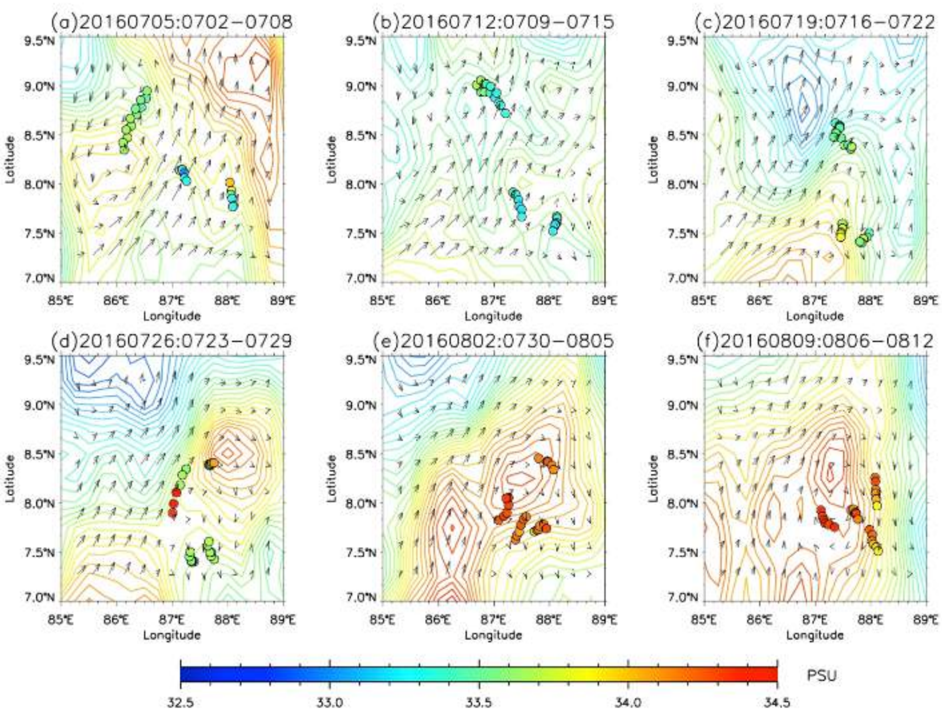

Figure 10. The Argo STS surface salinity data collected during BoBBLE field campaign from July 2 to August 12, 2016 are shown with SMAP L3 SSS for the same period. Each panel contains 7 days of STS data from four Argo floats (color circle) plotted on top of SMAP L3 SSS (color coded contours, offset by 0.4 PSU) and OSCAR currents (black arrows) for the corresponding week.

weekly SMAP SSS data, which is produced from SMAP L2 data for the same period. Also shown is the near surface ocean currents from OSCAR (Ocean Surface Current Analysis Real-time, available from http://podaac.jpl.nasa.gov). It appears that both SMAP and Argo depicted the salty water intrusion from Arabian Sea to the Bay of Bengal during the Indian Summer Monsoon. The surface salinity in the region jumped about 2 PSU in a few weeks when the salty water entered from the southern BOB in middle of July, transported northward, and spread over the region in early August. SMAP and Argo consistently captured the evolvement of rapid salinity change associated with the event. In the third week of July (Fig.10c), SMAP observed the sharp fronts of incoming salty water in southern BOB, when Argo floats happening to be near the fronts showed similar salinity values. The week after (Fig.10d), SMAP showed one patch of salty water moving northward, followed by a new patch of salty water input, while Argo floats situated in between the two patches. From late July to early August, the two patches merged when the floats were in the center of salinity maximum.

Figure 11 shows the scatter plots of collocated SMAP SSS and Argo salinity returned respectively by STS and 41-CP, which is averaged from measurements within 5 meters from surface. The comparison between SMAP and STS or 41-CP are quite similar with a standard deviation of about 0.2, RMSD of about 0.5 PSU and correlation exceeding 0.8. It is noted that the agreement with 41-CP is slightly better than STS. It should also be noted that a major part of RMSD is caused by a bias of about 0.45 PSU. We have examined the difference between SMAP and the RAMA buoy located at 8°N and 90°E, which is located slightly to the east of the domain indicated in Fig. 10; we found a small bias of 0.08 PSU at this RAMA buoy location (Fig. 12), much

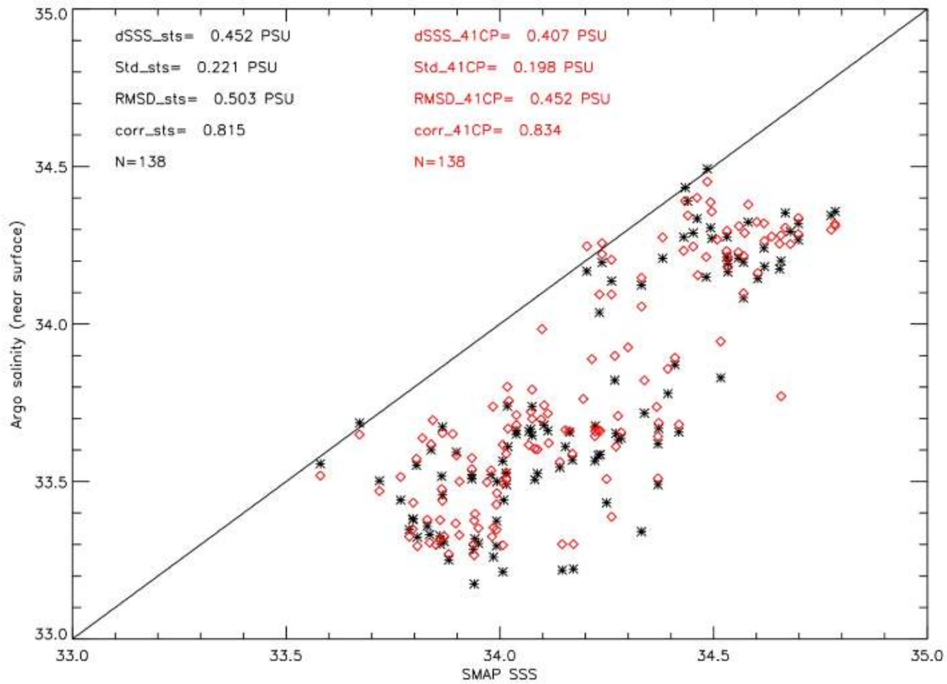

Figure 11. Scatter-plot of SMAP SSS and collocated Argo surface salinity from STS (black) and 41-CP (red).

smaller than the 0.5 PSU bias with respect to the STS or 41-CP. This suggests that there was a near surface salinity stratification with a horizontal gradient from east to west.

4. Conclusions

The SSS retrieved from the SMAP T_B has been validated with in situ measurements from Argo floats, moored buoys, and TSG data collected by ships on various time scales. We conclude that SMAP SSS retrieved from L-band radiometer has achieved an accuracy of 0.2 PSU globally between 40°S and 40°N on a monthly basis through comparison with Argo gridded data. In tropical oceans, salinity measured at 1 m by moored buoys indicate SMAP is able to track large salinity changes occurred within month, with RMSD of 0.26 PSU on weekly scale, which reduced to 0.22 PSU on monthly scale.

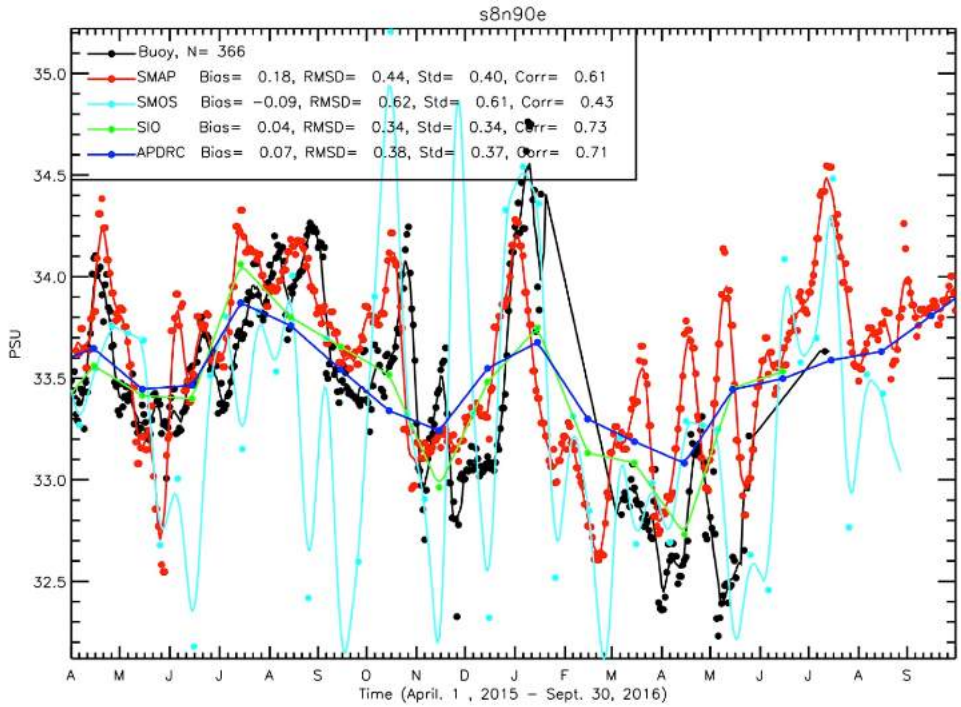

Figure 12. Time series of buoy salinity at 1m depth (black) and collocated SMAP (red) and SMOS (cyan) SSS at TAO buoy location 8°N, 90°E from April 1, 2015 to Sept. 30, 2016, with 7-day moving average applied, over plotted with monthly Argo data from SIO (green) and APDRC (blue).

The unique capability of SMAP to observe salinity signals in coastal oceans and marginal seas is demonstrated through an assessment using TSG data along ship tracks in the Mediterranean Sea and data collected from floats equipped with STS in BOB. SMAP reveals features consistent with the in situ measurements: the salinity spatial structure across the Mediterranean Sea, and sub-monthly evolution of Arabian salty water intrusion into BOB. The slightly higher RMSD (~0.5 PSU) observed in Mediterranean Sea and BOB may not only result from the land and RFI contamination on SSS retrieval, but also due to the limited number of matchups in these regions. A validation with the much more matchups of SMAP and in situ data, as well as process oriented studies such as demonstrated in Servain et a. [2016] are needed to provide systematic assessment of SMAP SSS retrieval in marginal seas and near coast.

The validation identified areas with relatively large discrepancy between SMAP and in situ measurements, suggesting future improvements of the T_B-only SMAP retrieval algorithm in the cold water, which tends to be under the influence of strong wind and high wave.

Note that the statistics of the differences of SMAP SSS from in-situ salinity measurements not only reflect the uncertainties of SMAP SSS, but also include other factors. These factors include (1) the uncertainties of the Argo IO products (e.g., Lee 2016), (2) near-surface salinity stratification (e.g., Boutin et al. 2015), and (3) scale-mismatch between averages on the satellite footprint and point-wise in-situ measurements (e.g., Vinogradova et al. 2013, Boutin et al. 2015).

Our time series comparison for SMAP, SMOS, Argo OI products, and mooring data suggest that the satellite SSS have the potential to be used for real-time QC of mooring salinity data to detect measurements that are significantly affected by issues such as biofouling. Satellites, Argo, moorings, and ships provide complementary platforms to monitor global ocean salinity and to assess the associated measurement and sampling errors from different platforms.

Acknowledgement

The work described in this paper was carried out by the Jet Propulsion Laboratory, California Institute of Technology under a contract with the National Aeronautics and Space Administration. Argo data were collected and made freely available by the International Argo Program and the national programs that contribute to it (http://www.argo.ucsd.edu, http://www.usgodae.org/argo/argo.html, http://argo.jcommops.org,). The Argo Program is part of the Global Ocean Observing

System. Moored buoy data are available from www.pmel.noaa.gov/tao. One of us (JM) acknowledge the support of the Spanish Ministry of Economy and Competitiveness, through the National R+D Plan under PROMISES Project ESP2015-67549-C3-2-R.

Reference

Bourlès, B., R. Lumpkin, M.J. McPhaden, F. Hernandez, P. Nobre, E. Campos, L. Yu, S. Planton, A. Busalacchi, A.D. Moura, J. Servain, and J. Trotte (2008). The PIRATA Program: History, Accomplishments, and Future Directions. *Bull. Amer. Meteor. Soc.*, 89, 1111-1125.

Boutin, J., Martin, N., Xiaobin, Y., Font, J., Reul, N., & Spurgeon, P. (2012). First assessment of SMOS data over open ocean: Part II; sea surface salinity. IEEE Transactions on Geoscience and Remote Sensing, 50(5), 1662–1675.

Boutin, J., et al. (2015). Satellite and in situ salinity: Understanding near-surface stratification and sub-footprint variability. Bulletin of the American Meteorological Society. http://dx.doi.org/10.1175/BAMS-D-15-00032.1.

Boutin, J., N. Martin, N. Kolodziejczyk, and G. Reverdin (2016). Interannual anoimalies of SMOS sea surface salinity. Remote Sensing of Environment 180, 128-136.

Entekhabi, D., E. G. Njoku, P. E. O'Neill, K. H. Kellogg, W. T. Crow, W. N. Edelstein, J. K. Entin, S. D. Goodman, T. J. Jackson, J. Johnson, J. Kimball, J. R. Piepmeier, R. D. Koster, N. Martin, K. C. McDonald, M. Moghaddam, S. Moran, R. Reichle, J. C. Shi, M. W. Spencer, S. W. Thurman, L. Tsang, and J. Van Zyl (2010). The Soil Moisture Active Passive (SMAP) Mission, Proceedings of IEEE, Vol. 98,No. 5,pp. 704-716.

Font, J., Camps, A., Borges, A., Martin-Neira, M., Boutin, J., Reul, N., ... Mecklenburg, S. (2010). SMOS: The challenging sea surface salinity measurement from space. Proceedings of the IEEE, 98(5), 649–665.

Fore, A., S. Yueh, W. Tang, B. Stiles, and A. Hayashi (2016). Combined Active/Passive Retrievals of Ocean Vector Wind and Sea Surface Salinity with SMAP, *IEEE Trans. Geoscience and Remote Sensing,* (??) doi: 10.1109/TGRS.2016.2601486.

Fournier, S., J. T. Reager, T. Lee, J. Vazquez-Cuervo, C. H. David, and M. M. Gierach, (2016). SMAP observes flooding from land to sea: The Texas event of 2015, Geophys. Res. Lett., 43, doi:10.1002/2016GL070821.

Freitag, H. P., M. E. McCarty, C. Nosse, R. Lukas, M. J. McPhaden, and M. F. Cronin (1999). COARE Seacat data: Calibrations and quality control procedures, NOAA Tech. Memo. ERL PMEL-115, 89 pp. [Available at http://www.pmel.noaa.gov/pubs/PDF/frei2034/frei2034.pdf.]

Kerr, Y. H., et al. (2010). The SMOS mission: New tool for monitoring key elements of the global water cycle. Proceedings of the IEEE, 98(5), 666–687.

Lagerloef, G., F. R. Colomb, D. Le Vine, F. Wentz, S. Yueh, C. Ruf, J. Lilly, J. Gunn, Y. Chao, A. deCharon, G. Feldman, and C. Swift (2008). The Aquarius/Sac-D Mission: Designed To Meet The Salinity Remote-Sensing Challenge, Oceanography, Vol. 21, no. 1, Special Issue: Sp. Iss. SI, pp. 68-81.

Larson, N. L., C. D. Janzen, and D. J. Murphy (2008). STS: An in- strument for extending ARGO temperature and salinity measurements through the sea surface. 2008 Ocean Sciences Meeting, Orlando, FL, American Society of Limnology and Oceanography. [Available online at http://www.seabird.com/

technical_references/SSalOceanSciencesMar08-5Pages.pdf.]

Le Vine, D. M., G. S.E. Lagerloef, F.R. Colomb, S.H. Yeh, and F.A. Pellerano (2007). Aquarius: An instrument to monitor sea surface salinity from space. *IEEE Trans. Geosci. Remote Sens.*, 45, 2040–2050.

Lee, T. (2016). Consistency of Aquarius sea surface salinity with Argo products on various spatial and temporal scales, Geophys. Res. Lett., 43, 3857–3864, doi:10.1002/2016GL068822.

Matthews, A. et al. (2015). BoBBLE: Bay of Bengal Boundary Layer Experiment. CLIVAR Exchanges No. 68, Vol. 19, No. 3, pp 38-42, Nov. 2015.

McPhaden, M. J. (1995). The TAO array is completed. *Bull. Amer. Meteor. Soc.*, 76, 739–741.

McPhaden, M.J., A.J. Busalacchi, R. Cheney, J.R. Donguy, K.S. Gage, D. Halpern, M. Ji, P. Julian, G. Meyers, G.T. Mitchum, P.P. Niiler, J. Picaut, R.W. Reynolds, N. Smith, K. Takeuchi (1998). The Tropical Ocean-Global Atmosphere (TOGA) observing system: A decade of progress. *J. Geophys. Res.*, 103, 14,169-14,240.

McPhaden, M.J., and Coauthors (2009). RAMA: The Research Moored Array for African–Asian–Australian Monsoon Analysis and Prediction. *Bull. Amer. Meteor. Soc.*, 90, 459–480.

Mohammed, P. N., M. Aksoy, J. R. Piepmeier, J. T. Johnson, and A. Bringer (2016). SMAP L-band Radiometer: RFI Mitigation Prelaunch Analysis and First Year On-Orbit Observations, IEEE Geosci. Remote Sens., Vo. 54, No. 10, pp. 6035-6047, Oct 2016, doi: 10.1109/TGRS.2016.2578048.

Roemmich, D., and the Argo Steering Team (2009). Argo: The challenge of continuing10 years of progress, Oceanography, 22, 46–55.

Servain, J., A. Busalacchi, M. McPhaden, A. Moura, G. Reverdin, M. Vienna, and S. Zebiak (1998). A Pilot Research Moored Array in the Tropical Atlantic (PIRATA). *Bull. Amer. Meteor. Soc.*, 79, 2019–2031.

Tang, W., S. Yueh, A. Fore, G. Neumann, A. Hayashi, and G. Lagerloef (2013). The rain effect on Aquarius' L-band sea surface brightness temperature and radar backscatter. *Remote Sensing of Environment*, 137, 147-157.

Tang, W., S. H. Yueh, A. G. Fore, and A. Hayashi (2014). Validation of Aquarius sea surface salinity with in situ measurements from Argo floats and moored buoys, J. Geophys. Res. Oceans, 119, 6171–6189, doi:10.1002/2014JC010101.

Tang, W., S. H. Yueh, A. Hayashi, A. G. Fore, W. L. Jones, A. Santos-Garcia, and M. M. Jacob (2015). Rain-induced near surface salinity stratification and rain roughness correction for Aquarius SSS retrieval. *The Special Issue of the IEEE Journal of Selected Topics in Applied Earth Observations and Remote Sensing (J-STARS)* "Aquarius/SACD mission calibration/validation performance and retrieval algorithms", 8 (12), 5474-5484, DOI: 10.1109/JSTARS.2015.2463768.

Tukey, J.W. (1977). Exploratory data analysis. Addison-Wesley.

Vinogradova, N. T., and R. M. Ponte (2013). Small-scale variability in sea surface salinity and implications for satellite-derived measurements, J. Atmos. Oceanic Technol., 30, 2689–2694, doi:10.1175/JTECH-D-13-00110.1.

Yueh, S. H., W. Tang, A. Fore, G. Neumann, A. Hayashi, A. Freedman, J. Chaubell, and G. Lagerloef (2013). L-band Passive and Active Microwave Geophysical Model Functions of Ocean Surface Winds and Applications to Aquarius Retrieval. *IEEE*

Trans. Geoscience and Remote Sensing, 51(9), 4619-4632, DOI: 10.1109/TGRS.2013.2266915.

Yueh, S. H., W. Tang, A. Fore, A. Hayashi, Y. T. Song, and G. Lagerloef (2014). Aquarius geophysical model function and combined active passive algorithm for ocean surface salinity and wind retrieval, *J. Geophys. Res. Oceans,* 119, 5360–5379, doi:10.1002/2014JC009939.

Yueh, S. H., A. Fore, W. Tang, A. Hayashi, B. Stiles, N. Reul, Y. Weng and F. Zhang (2016). SMAP L-Band Passive Microwave Observations Of Ocean Surface Wind During Severe Storms, *IEEE Trans. Geoscience and Remote Sensing,* doi: 10.1109/TGRS.2016.2600239.